The American Journal of Pathology, Vol. 193, No. 4, April 2023

The American Journal of
PATHOLOGY
ajp.amjpathol.org

VASCULAR BIOLOGY, ATHEROSCLEROSIS, AND ENDOTHELIUM BIOLOGY

Contribution of Hepatic Steatosis–Intensified Extracellular Vesicle Release to Aggravated Inflammatory Endothelial Injury in Liver-Specific *Asah1* Gene Knockout Mice

Xinxu Yuan,* Owais M. Bhat,* Yao Zou,* Yang Zhang,† and Pin-Lan Li*

From the Department of Pharmacology and Toxicology, Virginia Commonwealth University School of Medicine, Richmond, Virginia; and the Department of Pharmacological and Pharmaceutical Sciences,† College of Pharmacy, University of Houston, Houston, Texas*

Accepted for publication December 28, 2022.

Address correspondence to Pin-Lan Li, M.D., Ph.D., Department of Pharmacology and Toxicology, Medical College of Virginia, Virginia Commonwealth University, Richmond, VA 23298; or Yang Zhang, Ph.D., Department of Pharmacological and Pharmaceutical Sciences, College of Pharmacy, University of Houston, Houston, TX 77204-5037. E-mail: pin-lan.li@vcuhealth.org or yzhan219@central.uh.edu.

To study the mechanism by which nonalcoholic fatty liver disease (NAFLD) contributes to vascular endothelial Nod-like receptor pyrin domain 3 (NLRP3) inflammasome activation and neointima hyperplasia, NAFLD was established in high-fat diet (HFD)–treated *Asah1*$^{fl/fl}$/*Alb*^{cre} (liver-specific deletion of the acid ceramidase gene *Asah1*) mice. Compared with *Asah1* flox [*Asah1*$^{fl/fl}$/wild type (WT)] and wild-type (WT/WT) mice, *Asah1*$^{fl/fl}$/*Alb*^{cre} mice exhibited significantly enhanced ceramide levels and lipid deposition on HFD in the liver. Moreover, *Asah1*$^{fl/fl}$/*Alb*^{cre} mice showed enhanced expression of extracellular vesicle (EV) markers, CD63 and annexin II, but attenuated lysosome–multivesicular body fusion. All these changes were accompanied by significantly increased EV counts in the plasma. In a mouse model of neointima hyperplasia, liver-specific deletion of the *Asah1* gene enhanced HFD-induced neointima proliferation, which was associated with increased endothelial NLRP3 inflammasome formation and activation and more severe endothelial damage. The EVs isolated from plasma of *Asah1*$^{fl/fl}$/*Alb*^{cre} mice on HFD were found to markedly enhance NLRP3 inflammasome formation and activation in primary cultures of WT/WT endothelial cells compared with those isolated from WT/WT mice or normal diet–treated *Asah1*$^{fl/fl}$/*Alb*^{cre} mice. These results suggest that the acid ceramidase/ceramide signaling pathway controls EV release from the liver, and its deficiency aggravates NAFLD and intensifies hepatic EV release into circulation, which promotes endothelial NLRP3 inflammasome activation and consequent neointima hyperplasia in the mouse carotid arteries. *(Am J Pathol 2023, 193: 493–508; https://doi.org/10.1016/j.ajpath.2022.12.007)*

Nonalcoholic fatty liver disease (NAFLD) is one of the most common chronic liver diseases around the world, especially in the Western nations. In the United States, it affects about 25% of the population.[1] NAFLD is an umbrella term for a range of liver conditions affecting people who drink little or no alcohol. The major characteristic of NAFLD is the overaccumulation of fat in the liver cells. NAFLD ranges from hepatic steatosis (fatty liver) to nonalcoholic steatohepatitis with inflammation and hepatocellular injury or fibrosis, to advanced fibrosis and cirrhosis, and in some cases, carcinoma.[2] Not only does the adverse effect of NAFLD confines to the progression of deteriorating liver function, but also accumulating evidence has shown a strong link between NAFLD and cardiovascular diseases (CVDs), including valve disease, aneurysm, cardiac arrhythmia, heart failure, cardiomyopathy, and pericarditis, especially for the coronary artery disease, including heart attack, stroke, and angina.[3] However, whether NAFLD is a marker or an independent risk factor that promotes cardiovascular disease remains controversial.[4]

NAFLD drives multiple potential mechanisms, leading to cardiovascular disease. These mechanisms include systemic

Supported by NIH grants HL057244 (P.-L.L.), HL075316 (P.-L.L.), HL122937 (Y.Z. and P.-L.L.), and DK120491 (P.-L.L.).
Disclosures: None declared.

https://doi.org/10.1016/j.ajpath.2022.12.007

inflammation, lipid metabolism, oxidative stress, systemic insulin resistance, as well as microbiota symbiosis, which may also be influenced by other factors, such as genetic and epigenetic variations.[5] In patients with NAFLD, the level of asymmetrical dimethylarginine, an endogenous inhibitor of nitric oxide synthase and homocysteine, is increased, which stimulates platelet activation and induces more inflammation factors, finally leading to endothelial dysfunction and altered vascular tone as well as plague formation.[6,7] In patients with NAFLD, triglyceride, very low-density lipoprotein, and low-density lipoprotein levels as well as liver fat are increased, but high-density lipoprotein levels are decreased, which causes the increase of free fatty acid and hepatic inflammation, resulting in dysfunction of lipid metabolism.[8] Moreover, NAFLD is also closely associated with insulin resistance, which increases hepatic diacylglycerol, resulting in decreased insulin signaling.[9] Fatty acid accumulation in the liver, primarily from adipose tissue, also leads to a decrease of liver glucose, further stimulating insulin resistance.[10] At the same time, factors such as homocysteine, insulin resistance, and fatty acid accumulation induce oxidative stress, which causes endothelial dysfunction.[11] When NAFLD proceeds to fibrosis, angiogenesis is active and vascular endothelial growth factor as well as vascular endothelial growth factor receptor 2 increase, which influences atherogenesis and plaque instability.[12] Intestinal dysbiosis and bile acids, as well as trimethylamine and short-chain fatty acids, also contribute to atherosclerosis.[13] Despite many mechanisms being proposed, the exact mechanisms by which NAFLD causally contributes to CVDs are not fully elucidated.

The link between NAFLD and CVDs suggests that intercellular communication is important for the pathogenic process of diseases.[14] In recent years, it is well recognized that cell communication occurs not only via direct contact and soluble factors but also via extracellular vesicles (EVs).[15] EVs are lipid bilayer-enclosed nanoparticles released by cells, and play an important role in local and distant intercellular communications.[16] On the basis of the size difference, EVs have been categorized into exosomes (30 to 150 nm), microvesicles (100 to 1000 nm), and apoptosis bodies (50 to 5000 nm), which carry cargo such as proteins, lipids, RNAs, DNAs, and other components.[17] Recently, hepatocyte-derived EVs were reported to promote endothelial inflammation and atherogenesis via miRNA-1, which suggests that hepatocyte-derived EVs may play an important role in NAFLD-induced CVDs.[14] Hepatic small EVs also promote microvascular endothelial hyperpermeability during NAFLD via novel miRNA-7.[18] However, the regulation of lysosomal ceramide on hepatocyte-derived EV release and hepatic steatosis—induced endothelial Nod-like receptor pyrin domain 3 (NLRP3) inflammasome activation and neointima formation are still poorly explored.

Ceramides play an important role in liver systemic inflammation, lipid metabolic insulin resistance, and oxidative stress, which are involved in NAFLD-induced CVDs.[19] Jiang et al[20] have reported that inhibiting ceramide synthesis attenuates hepatic steatosis and fibrosis in rats with NAFLD. Kasumov et al[21] have also reported that ceramide mediates NAFLD and is associated with atherosclerosis. Recent studies have demonstrated that lysosomal ceramide directly contributes to kidney[22,23] or cardiovascular diseases.[24,25] However, whether lysosomal ceramide contributes to NAFLD-induced CVDs is not known.

The present study hypothesized that lysosomal ceramide mediates hepatocyte-derived EV release, which contributes to hepatic steatosis—induced endothelial inflammasome activation and neointima formation. To test this hypothesis, first, whether loss of acid ceramidase (AC; encoded by *Asah1* gene) function caused the abnormal ceramide metabolism and aggravated hepatic steatosis was examined in liver-specific *Asah1* gene knockout ($Asah1^{fl/fl}/Alb^{cre}$) mice. Then, whether such abnormal ceramide metabolism contributed to the increased hepatic EV release into the plasma was studied. Whether the increased release of hepatic EVs due to acid ceramidase deficiency in the liver was associated with enhanced endothelial NLRP3 inflammasome and neointima formation in the carotid arterial wall of mice was explored next. Finally, whether the isolated EVs from steatotic mice could directly induce NLRP3 inflammasome activation in cultured endothelial cells (ECs) was tested. The results suggest that acid ceramidase controls EV release from the liver, and its deficiency intensifies NAFLD and thereby releases more EVs to promote endothelial NLRP3 inflammasome activation and consequent neointima proliferation.

Materials and Methods

Mice

All procedures were performed following the NIH *Guide for the Care and Use of Laboratory Animals*.[26] All animal experiments were approved by the Institutional Animal Care and Use Committee of Virginia Commonwealth University. Male and female C57BL/6J wild-type (WT)/WT, $Asah1^{fl/fl}$/WT, and $Asah1^{fl/fl}/Alb^{cre}$ mice (aged 8 to 12 weeks; weight, 18 to 23 g) were produced for all the experiments. All mice were housed in a controlled environment at 20 ± 2°C and 40% to 50% humidity, with a 12-hour light/12-hour dark cycle with free access to food and water. Mice were separated into six groups randomly and fed with the normal diet (ND) or high-fat diet (HFD; 60% fat) for 10 weeks. All mice used in the *in vivo* studies were genotyped for the $Asah1^{fl/fl}/Alb^{cre}$ and Cre recombinase gene to confirm liver-specific gene deletion of acid ceramidase α subunit. Briefly, genomic DNA extracted from the tail was subjected to PCR amplification using Taq DNA polymerase (Invitrogen Inc., Grand Island, NY). PCR was performed using a validated protocol provided by Jackson Laboratory (Bar Harbor, ME). The $Asah1^{fl/fl}/Alb^{cre}$ mice were detected using primers of 5′-ACAACTGTGTAGGATT-CACGCATTCTCC-3′ (forward) and 5′-TCGA

TCTAT-GAAATGTCGCTGTCGG-3′ (reverse). The internal control (AC Extron) was detected using primers of 5′-CTAGGCCACA-GAATTGAAAGATCT-3′ (forward) and 5′-GTAGGTG-GAAATTCTAGCATCATCC-3′ (reverse). The Cre recombinase gene was detected using primers of 5′-CTAGGCCACAGAATTGAAAGATCT-3′ (forward) and 5′-GTAGGTGGAAATTCTAGCATCATCC-3′ (reverse). The PCR products were separated by gel electrophoresis on a 3% agarose gel, visualized by ethidium bromide fluorescence, and compared with a 100-bp DNA ladder (New England Biosystems, Ipswich, MA). To further identify *Asah1*$^{fl/fl}$/*Alb*^{cre} mice, B6.129-Gt(ROSA)26Sortm1Joe/J (ROSA) mice were crossbred with *Asah1*$^{fl/fl}$/*Alb*^{cre} mice to generate *Asah1*$^{fl/fl}$/*Alb*^{cre}/ROSA mice.

Partial Ligated Carotid Artery

The surgery of the partial ligated carotid artery (PLCA) was conducted as previously reported.[27,28] First, 2% isoflurane inhalation was used for 5 minutes to anesthetize the mice, and the hair in the neck was epilated. Then, the mice were kept anesthetized through a nose cone. After sterilization with a tincture of iodine, a ventral midline incision was made in the neck, and the muscle layers were separated with curved forceps to expose the left carotid artery. The external carotid, internal carotid, and occipital artery, except for the superior thyroid artery, were ligated with a piece of 6.0 silk suture, which will provide the sole source of blood circulation. The unligated right carotid artery served as an internal control. Next, the incision and disinfection were performed, then the mice were kept on a heating pad until they gained consciousness. The mice were sacrificed after 4 weeks of PLCA, and both of their carotid arteries were isolated for frozen sections and paraffin sections. The slides were used for immunohistochemistry, dual-fluorescence staining, and confocal analysis.

Morphologic Examination and Medial Thickening Analysis

Morphologic changes were measured by hematoxylin and eosin staining, as described previously.[29] Briefly, after perfusion with cold phosphate-buffered saline (PBS) for 5 minutes, carotid arteries were isolated and immersed into 10% neutral-buffered formalin. Then, the carotid artery was embedded in paraffin and cut into serial sections (7 μm thick) for histopathologic evaluation. For hematoxylin and eosin staining, the sections were heated for 10 minutes at 65°C and deparaffinized twice in 100% xylene for 10 minutes. Next, the samples were rehydrated with 100%, 95%, 75%, and 50% ethanol in the water. After that, the sections were immersed in hematoxylin for another 10 minutes. Once the color turned to blue, the sections were stained with eosin for another 10 minutes. Next, the sections were rinsed with running water and dehydrated with different grades of ethanol. Finally, dibutyl phthalate polystyrene xylene was used to mount the slides. Intimal-medium thickening of carotid arteries was examined using Image-Pro Plus software version 6.0 (Media Cybernetics Inc., Bethesda, MD).

Immunofluorescence Staining

Primary cultured ECs in 8-well plates or carotid arteries on frozen slides were rinsed once for 5 minutes with PBS and fixed with 4% paraformaldehyde in PBS for 15 minutes at room temperature. After being washed two to three times with PBS (Fisher Scientific, Hampton, NH) for 5 minutes, the samples were permeabilizated with 0.1% Triton X-100 in PBS for 10 minutes and were washed two to three times for 5 minutes with PBS. Then, samples were incubated with a primary antibody overnight at 4°C, followed by incubation with either Alexa-488− or Alexa-555−labeled secondary antibody (Invitrogen, Carlsbad, CA; 1:200) for 1 hour at room temperature in the darkroom. Primary antibody dilution and catalog information are as follows: AC$^{\alpha}$ (1:200; LS-B11969; LSBio, Seattle, WA), albumin (1:500; AF3329; R&D Systems, Minneapolis, MN), lysosomal-associated membrane protein-1 (1:200; MAB4320; R&D Systems), Cre (1:500; ab24607; Abcam, Cambridge, MA), vacuolar protein sorting-associated protein 16 homolog (VPS16; 1:300; 17776-1-AP; Proteintech, Rosemont, IL), NLRP3 (1:200; MAB7578; R&D Systems), apoptosis-associated speck-like protein containing a caspase-recruitment domain (ASC; 1:200; catalog number SAB4501314; Santa Cruz Biotechnology, Dallas, TX), caspase-1 (1:200; SC-392736; Santa Cruz Biotechnology), and von Willebrand factor (vWF; 1:300; ab11713; Abcam). Finally, the slides were mounted using the mounting medium with DAPI and sealed with nail polish for taking pictures using a confocal laser scanning microscope (Fluoview FV1000; Olympus, Tokyo, Japan). Cell- or tissue-specific staining intensity was measured and analyzed with ImageJ software version 1.53e (NIH, Bethesda, MD; *http://imagej.nih.gov/ij*, last accessed December 30, 2022). The colocalization of NLRP3 (Abcam) with ASC (Santa Cruz Biotechnology) or caspase-1 (Santa Cruz Biotechnology; 1:200) was analyzed by the Image-Pro Plus software version 6.0. These summarized colocalization efficiency data were expressed as Pearson correlation coefficient, as described previously.[30,31]

Immunohistochemistry

To perform the immunohistochemistry, paraffin sections were made using fixed mouse carotid arteries in 10% formalin, where tissues were dehydrated and embedded in paraffin and cut into sections (7 μm thick). Immunohistochemical examinations were performed according to the manufacturer's protocol for CHEMICAL IHC Select HRP/DAB Kit (EMD Millipore, Burlington, MA). Briefly, antigen was recovered with citrate buffer at 100°C for 15 minutes, and endogenous peroxidase activity was quenched with 3% H_2O_2 for 15 minutes at room temperature.

Then, 2.5% horse serum was used to block the non-specific antibodies for 1 hour at room temperature, followed by incubation with primary antibodies CD63 (1:200; NBP2-32830; NOVUS, Centennial, CO), annexin II (1:200; catalog number SC-9061; Santa Cruz Biotechnology), ceramide (1:200; ALX-804-196; Enzo, Farmingdale, NY), Cre (1:200; ab216262; Abcam), and IL-1β (1:200; P420B; Invitrogen; Waltham, MA), overnight at 4°C and subsequently with biotinylated secondary antibodies and a streptavidin peroxidase complex (PK-7800; Vector Laboratories, Burlingame, CA) for 30 minutes. Finally, the tissues were counterstained with hematoxylin, dehydrated, and mounted using dibutyl phthalate polystyrene xylene. The area percentage of the positive staining was measured using Image-Pro Plus software version 6.0.[32]

In Situ Analysis of Caspase-1 Activity

Caspase-1 activity was performed, as described previously.[33] This assay uses fluorescent-labeled inhibitor of caspases (FLICA) probes (Immunochemistry Technologies, LLC, Bloomington, MN) to label activated caspase-1 enzyme in the arterial endothelium. FLICA probe is composed of a caspase-1 recognition sequence, tyrosine−valine−alanine−aspartic acid (YVAD), which binds to active caspase-1, a fluoromethyl ketone (FMK) moiety that results in irreversible binding with the enzyme, and a fluorescent tag FAM (carboxyfluorescein) reporter. After entering the cells, the FLICA reagent FAM-YVAD-FMK becomes covalently coupled to the active caspase-1, whereas any unbound FLICA reagent diffuses out of the cell and is washed away. The remaining green fluorescent signal is a direct measure of the active caspase-1 enzyme activity in the cell or tissue samples. To detect caspase-1 activity in the arterial endothelium, frozen section slides were first fixed in 100% acetone for 15 minutes and incubated overnight at 4°C with sheep anti-vWF (1:200; Abcam). These slides were then costained with fluorescence-conjugated anti-sheep secondary antibody and FLICA reagent (1:10) from a FLICA Caspase 1 Assay Kit (Immunochemistry Technologies, LLC) for 1.5 hours at room temperature. Colocalization was analyzed by Image-Pro Plus software. The colocalization coefficient was represented by Pearson correlation coefficient.

Isolation and Purification of Extracellular Vesicles

Differential ultracentrifugation was used to isolate the EVs, as previously described.[34,35] Briefly, the medium or plasma was collected and spun (300 × *g*) at 4°C for 10 minutes to remove detached cells or debris. Apoptotic bodies, microvesicles, and cell debris were removed after being filtered through 0.22-μm filters. EVs in the supernatant were spun down by ultracentrifugation at 100,000 × *g* for 120 minutes at 4°C (70.1 T1 ultracentrifuge rotator; Beckman, Indianapolis, IN). After washing in ice-cold filtered PBS, EVs were resuspended in 100 μL ice-cold filtered PBS. CD63 Exo-Flow Capture Kit (EXOFLOW300A-1; System Biosciences, Palo Alto, CA) was used for purification and characterization.

Nanoparticle Tracking Analysis

Nanoparticle tracking analysis was used to characterize EVs with the light scattering mode of the NanoSight LM10 (NanoSight Ltd., Amesbury, UK). Five frames (30 seconds each) were captured for each sample with background level 10, camera level 12, and shutter speed 30. Captured EV distribution images were analyzed using NanoSight NTA software version 3.2, build 16. EVs isolated from plasma were diluted (1:1000) before analysis. Particle size, ranging between 40 and 200 nm, was calculated.

Cell Culture

Isolation of mouse carotid arterial ECs was performed and characterized, as previously described.[36,37] ECs were primed with a low dose of lipopolysaccharide (1 ng/mL) for 3 hours before any experiments. Then, ECs were treated with EVs isolated from ND- or HFD-treated mouse plasma for 24 hours.

Western Blot Analysis

Western blot analysis was performed, as previously described.[38] Briefly, total protein was extracted using lysis buffer after being washed in cold PBS. Protein concentrations were measured and resuspended to 2 μg/μL. Cell lysates were run on an SDS-PAGE gel at a voltage of 100 V for 2 to 3 hours. Protein was transferred into a polyvinylidene difluoride membrane at the voltage of 100 V for 1 hour. Non-specific proteins were blocked with 5% nonfat milk in tris-buffered saline with Tween 20 buffer for 30 minutes. Then, the membrane was incubated with primary antibodies against pro−caspase-1 (1:500; SC-56036; Santa Cruz Biotechnology), cleaved caspase-1 (1:500 dilution; SC-514; Santa Cruz Biotechnology), CD63 (1:500; NBP2-32830; NOVUS), CD81 (1:500; SC-9158; Santa Cruz Biotechnology), CD9 (1:500; SC-52519; Santa Cruz Biotechnology), and cytochrome P450 2E1 (CYP2E1; 1:2000; ab28146; Abcam) overnight at 4°C, followed by incubation with a secondary antibody labeled with horseradish peroxidase for 1 hour at room temperature. The membrane was developed with Kodak Omat film (IB1660760; VWR, Radnor, PA) after being washed three times with tris-buffered saline with Tween 20. β-Actin (1:8000 dilution; Santa Cruz Biotechnology) was reported to serve as a loading control. The intensity of the bands was quantified using NIH ImageJ software version 1.53e (*http://imagej.nih.gov/ij*, last accessed December 30, 2022).

Enzyme-Linked Immunosorbent Assay Analysis of IL-1β Secretions

The culture medium was collected for IL-1β quantification with an IL-1β enzyme-linked immunosorbent assay kit

(R&D Systems), according to the manufacturer's instructions and previous studies.[39] In brief, 200 μL of the culture medium was added to a microplate strip well and incubated for 2 hours at room temperature. Then, the solution was mixed with IL-1β conjugate and incubated for another 2 hours at room temperature. Thorough washes were performed between and after the two incubations. A total of 100 μL of substrate solution was applied to generate chemiluminescence. Chemiluminescent absorbance was determined using a microplate reader at $\lambda = 450$. The IL-1β level was quantified by relating the sample readings to the generated standard curve.

X-Gal Staining

LacZ Staining Kit (Rep-lz-c; Invivogen, San Diego, CA) was used to identify *Asah1*$^{fl/fl}$/*Alb*^{cre}/ROSA mice. In brief, liver frozen sections were fixed with fixative solution at room temperature for 10 minutes. The sections were rinsed twice with PBS, and staining solutions were added. The sections were incubated at 37°C overnight in the wet box. Finally, the sections were checked under a microscope for the development of blue color, and images were taken.

Statistical Analysis

Data are presented as means ± SEM. Significant differences between the two groups of experiments were examined using the *t*-test. Significant differences between and within multiple groups were examined using analysis of variance for repeated measures, followed by the Duncan multiple range test. The statistical analysis was performed by Sigmaplot 12.5 software (Systat Software, San Jose, CA). $P < 0.05$ was considered statistically significant.

Results

Characterization of *Asah1*$^{fl/fl}$/*Alb*^{cre} Mice

Asah1$^{fl/fl}$/*Alb*^{cre} mice were generated by crossing the *Asah1* floxed mice (*Asah1*$^{fl/fl}$) with B6.Cg-Speer6-ps1Tg (*Alb*-Cre) 21Mgn/J (stock number 003574 | Albumin-Cre) from the Jackson Laboratory. Deletion of the *Asah1* gene (AC$^{\alpha}$) and transgene of Cre was verified by PCR analysis. As shown in Figure 1A, *Asah1*$^{fl/fl}$/*Alb*^{cre} mice had two positive PCR products, including 175 bp for Cre and 585 bp for floxed *Asah1* gene. *Asah1*$^{fl/fl}$/WT mice had positive floxed *Asah1* gene (585 bp), but no Cre (175 bp). WT/WT mice had wild-type *Asah1* genes (482 bp), but not floxed *Asah1* and Cre genes. Cre-mediated liver-specific recombination was also validated by breeding the *Asah1*$^{fl/fl}$/*Alb*^{cre} mice with ROSA double reporter mice to produce an *Asah1*$^{fl/fl}$/*Alb*^{cre}/ROSA strain. ROSA mice carry a floxed blocker of the reporter gene, enhanced green fluorescent protein. Cre excision of the blocker in *Asah1*$^{fl/fl}$/*Alb*^{cre}/ROSA mice activated enhanced green fluorescent protein to produce green fluorescence, as detected by *in vivo* imaging in the mouse and the dissected liver (Figure 1B). X-Gal staining indicated blue color for live cells, as shown in Supplemental Figure S1. Using immunochemistry staining, a significant decrease in the AC protein was observed in the liver of *Asah1*$^{fl/fl}$/*Alb*^{cre} mice with Cre expression, which resulted in the accumulation of ceramide, as shown by remarkedly increased ceramide expression in the liver of *Asah1*$^{fl/fl}$/*Alb*^{cre} mice (Figure 1C). Moreover, confocal microscopy failed to indicate AC protein in the liver and lysosomes of *Asah1*$^{fl/fl}$/*Alb*^{cre} mice, as shown by the colocalization of AC$^{\alpha}$ with *Alb* as a liver marker or lysosomal-associated membrane protein-1 as a lysosomal marker. However, AC$^{\alpha}$ was detected in the liver of WT/WT and *Asah1*$^{fl/fl}$/WT mice (Figure 1D). In contrast, Cre was only detected in the liver of *Asah1*$^{fl/fl}$/*Alb*^{cre} mice, as shown by the colocalization of Cre with *Alb* (Figure 1D). These results confirmed that the *Asah1* gene was deleted in the hepatocytes of *Asah1*$^{fl/fl}$/*Alb*^{cre} mice.

Intensified Hepatic Steatosis in the Liver of *Asah1*$^{fl/fl}$/*Alb*^{cre} Mice with HFD

It is known that ceramide regulates NAFLD[20]; therefore, first, the effects of *Asah1* gene deletion on ceramide expression and hepatic steatosis on the HFD were confirmed. As shown in Figure 2, A and B, using immunohistochemistry staining, increased ceramide expression in WT/WT or *Asah1*$^{fl/fl}$/WT mice on the HFD was observed in the liver, and the increase was markedly enhanced by *Asah1* gene deletion in *Asah1*$^{fl/fl}$/*Alb*^{cre} mice. *Asah1*$^{fl/fl}$/*Alb*^{cre} mice on the HFD had elevated HFD-induced lipid deposition in the liver as indicated by hematoxylin and eosin staining and Oil Red staining compared with the littermates of WT/WT or *Asah1*$^{fl/fl}$/WT mice, as shown by the representative and summarized data in Figure 2, C through F. These results suggest that *Asah1* gene deletion or ceramide accumulation in the liver regulates HFD-induced hepatic steatosis.

Enhanced EV Release and Impaired Interaction of Multivesicular Bodies with Lysosomes in the Liver of *Asah1*$^{fl/fl}$/*Alb*^{cre} Mice

The interaction of lysosomes with multivesicular bodies (MVBs) plays an important role in MVB-regulated EV fate.[40] Given that AC$^{\alpha}$ is mainly detected in the lysosome and its action on lysosome trafficking or function,[41,42] the effect of *Asah1* gene deletion on EV secretion in the liver was examined. As shown in Figure 3, A through D, using immunochemistry staining, EV markers, CD63 and annexin II, were detected in the liver of mice on the HFD. *Asah1* gene deletion in *Asah1*$^{fl/fl}$/*Alb*^{cre} mice notably increased CD63 and annexin II expression, even in those on the ND diet. Moreover, HFD treatment also significantly increased CD63 and annexin II expression in the liver of WT/WT mice and *Asah1*$^{fl/fl}$/WT mice, which was enhanced by the *Asah1* gene deletion in the liver of *Asah1*$^{fl/fl}$/*Alb*^{cre} mice. Furthermore, using Nanosight, a

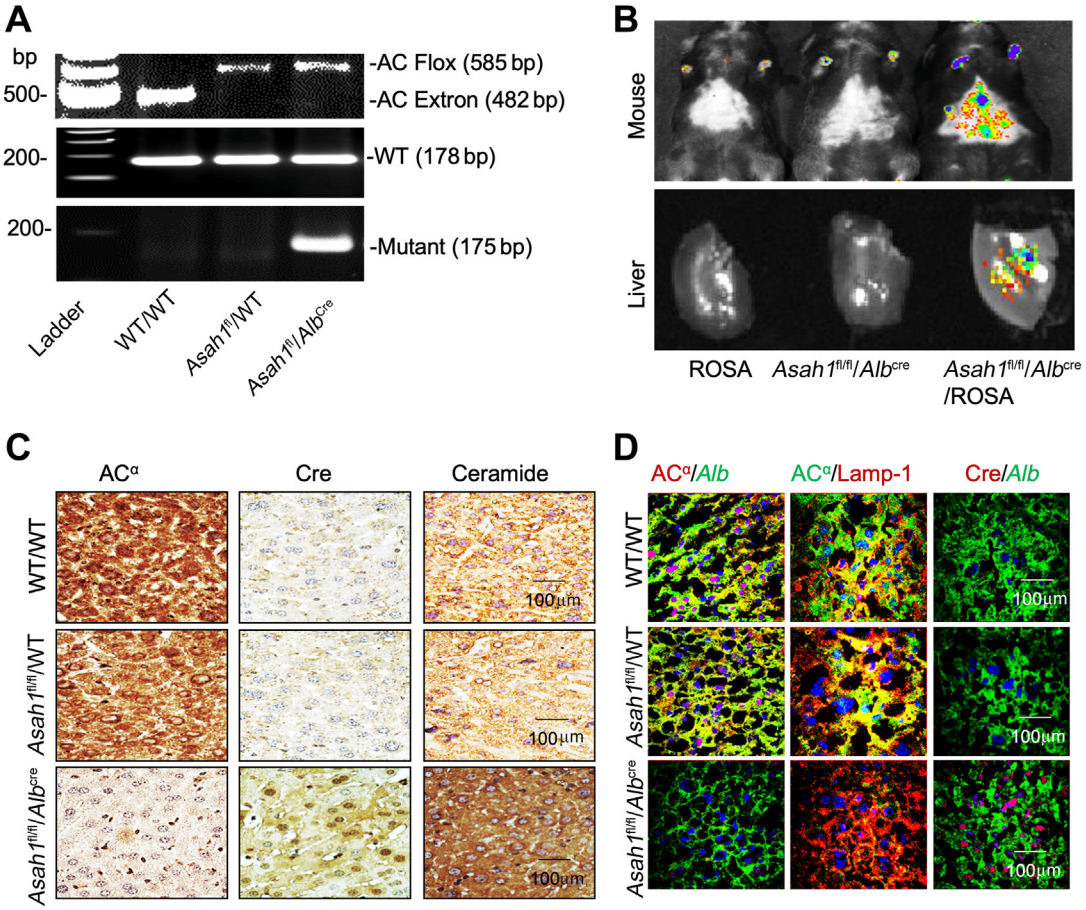

Figure 1 Characterization of liver-specific *Asah1* knockout mice (*Asah1*$^{fl/fl}$/*Alb*^{cre}). **A:** Wild type (WT)/WT has two positive PCR products, including Cre recombinase (Cre) at 178 bp and floxed *Asah1* at 482 bp. *Asah1*$^{fl/fl}$/WT has two positive PCR products, including Cre at 178 bp and floxed *Asah1* at 585 bp. *Asah1*$^{fl/fl}$/*Alb*^{cre} has three positive PCR products, including Cre at 178 and 175 bp and floxed *Asah1* at 585 bp. **B:** Cre-mediated endothelial cell–specific recombination was validated by breeding the *Asah1*$^{fl/fl}$/*Alb*^{cre} mice with B6.129-Gt(ROSA)26Sortm1Joe/J (ROSA) reporter mice; *in vivo* and *ex vivo* imaging of the offspring shows green fluorescent protein expression in the mice and liver. **C:** Representative immunohistochemistry staining, showing acid ceramidase (AC) and Cre protein as well as Cre protein expression in the liver of *Asah1*$^{fl/fl}$/*Alb*^{cre} mice and their littermate WT/WT and *Asah1*$^{fl/fl}$/WT mice. **D:** Representative fluorescent confocal microscopy images showing the colocalization of a subunit of AC (AC$^{\alpha}$) versus *Alb*, AC$^{\alpha}$ versus lysosomal-associated membrane protein-1 (Lamp-1), and *Alb* versus Cre, indicating AC$^{\alpha}$ protein only expression in the hepatocytes and the lysosomes of WT/WT and *Asah1*$^{fl/fl}$/WT mice but not expression in *Asah1*$^{fl/fl}$/*Alb*^{cre} mice. There were at least three mice in each group. $n = 3$ (**A**–**D**). Scale bars = 100 μm (**C** and **D**).

nanoparticle tracking analyzer, it was found that plasma-derived EVs were significantly increased in WT/WT mice and *Asah1*$^{fl/fl}$/WT mice fed on the HFD compared with the ND. The increase was markedly enhanced by the *Asah1* gene deletion in *Asah1*$^{fl/fl}$/*Alb*^{cre} mice on the HFD. However, no significant change was observed due to *Asah1* gene deletion in *Asah1*$^{fl/fl}$/*Alb*^{cre} mice fed on the ND compared with ND-treated WT/WT mice and *Asah1*$^{fl/fl}$/WT mice, as shown in Figure 3E by a summarized bar graph of EV relative concentration in the mice plasma. Interestingly, the colocalization of lysosomal-associated membrane protein-1 versus VPS16 was significantly decreased in WT/WT mice and *Asah1*$^{fl/fl}$/WT mice, as shown by the yellow spots, after HFD as compared with ND. *Asah1* gene deletion decreased the colocalization of lysosomal-associated membrane protein-1 in *Asah1*$^{fl/fl}$/*Alb*^{cre} mice on ND versus VPS16 compared with their littermates. In addition, attenuated HFD-induced decrease in colocalization of these markers in the WT/WT mice and *Asah1*$^{fl/fl}$/WT mice was further attenuated by *Asah1* gene deletion (Figure 3, F and G). The data indicate that *Asah1* gene deletion impairs the fusion of lysosomes with MVBs, which leads to enhanced EV release.

Aggravated Endothelial NLRP3 Inflammasome Activation in the Carotid Arteries by *Asah1* Gene Deletion in the Liver of *Asah1*$^{fl/fl}$/*Alb*^{cre} Mice

The NLRP3 inflammasome formation in PLCAs was analyzed by examining the colocalization of NLRP3 inflammasome components using confocal immunofluorescence microscopy (Figure 4). As shown in Figure 4, A and C, in WT/WT or *Asah1*$^{fl/fl}$/WT control mice, HFD significantly increased the colocalization of NLRP3 versus ASC or caspase-1 compared with the ND, as shown by yellow spots in the intima of the

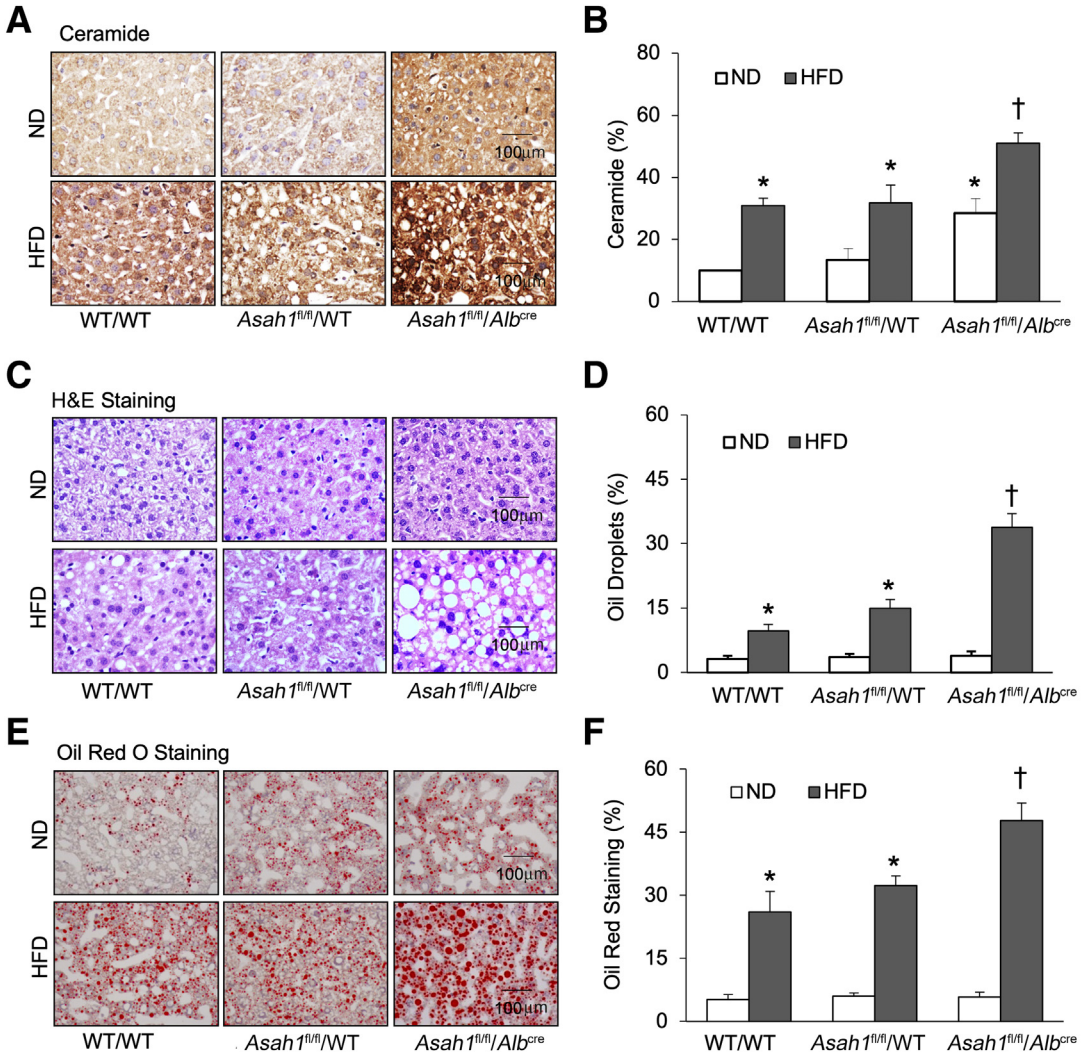

Figure 2 Enhanced hepatic steatosis by *Asah1* gene deletion in the liver of *Asah1*$^{fl/fl}$/*Alb*^{cre} mice on the high-fat diet (HFD). **A:** Representative immunohistochemistry staining showing the accumulation of ceramides in the liver of *Asah1*$^{fl/fl}$/*Alb*^{cre} mice and their littermate controls, wild-type (WT)/WT or *Asah1*$^{fl/fl}$/WT mice, on the normal diet (ND) or HFD. **B:** Summarized data showing the intensity of ceramide in the liver with an anti-ceramide antibody. **C** and **E:** Representative hematoxylin and eosin (H&E) staining and Oil Red O staining showing the accumulation of lipid droplets in the liver. **D** and **F:** Summarized data showing the percentage of positive lipid droplets in the liver. Data are expressed as means ± SEM (**B**, **D**, and **F**). $n = 5$ (**A**–**F**). *$P < 0.05$ versus WT/WT-ND or *Asah1*$^{fl/fl}$/WT-ND group; $^{\dagger}P < 0.05$ versus WT/WT–Western diet (WD) or *Asah1*$^{fl/fl}$/WT-HFD group. Scale bars = 100 μm (**A**, **C**, and **E**).

carotid arteries. The HFD-induced increase in the colocalization of NLRP3 components was enhanced in *Asah1*$^{fl/fl}$/*Alb*^{cre} mice compared with WT/WT or *Asah1*$^{fl/fl}$/WT mice. The quantified colocalization coefficient data are summarized in Figure 4, B and D. In addition to their formation, the activation of the NLRP3 inflammasome was analyzed by testing the caspase-1 activity using FLICA probes (Figure 4, E and F) and IL-1β expression using immunohistochemistry staining (Figure 4, G and H). As shown in Figure 4, E and F, there was no significant colocalization of FLICA with endothelial marker vWF in all mouse strains on ND, suggesting a basal level of NLRP3 inflammasome activity in these mice. In contrast, HFD significantly increased the FLICA/vWF colocalization in WT/WT and *Asah1*$^{fl/fl}$/WT control mice, which was significantly enhanced in *Asah1*$^{fl/fl}$/*Alb*^{cre} mice. Accompanied by enhanced caspase-1 activity by HFD, *Asah1*$^{fl/fl}$/*Alb*^{cre} mice showed a more significant increase in the levels of IL-1β expression by HFD in the carotid intima region compared with that in WT/WT and *Asah1*$^{fl/fl}$/WT mice (Figure 4, G and H). Together, these data suggest that *Asah1* gene deletion in the liver enhances endothelial NLRP3 inflammasome formation and activation in the carotid arteries of mice.

Augmented Neointima Formation and Endothelial Injury in the Carotid Arteries by *Asah1* Gene Deletion in the Liver of *Asah1*$^{fl/fl}$/*Alb*^{cre} Mice

The neointima formation as a major pathologic change in PLCA was also analyzed in *Asah1*$^{fl/fl}$/*Alb*^{cre} mice and their littermates on the ND and HFD by hematoxylin and eosin staining. As shown in Figure 5A, the neointima formation was not observed in PLCAs of *Asah1*$^{fl/fl}$/*Alb*^{cr} mice on ND

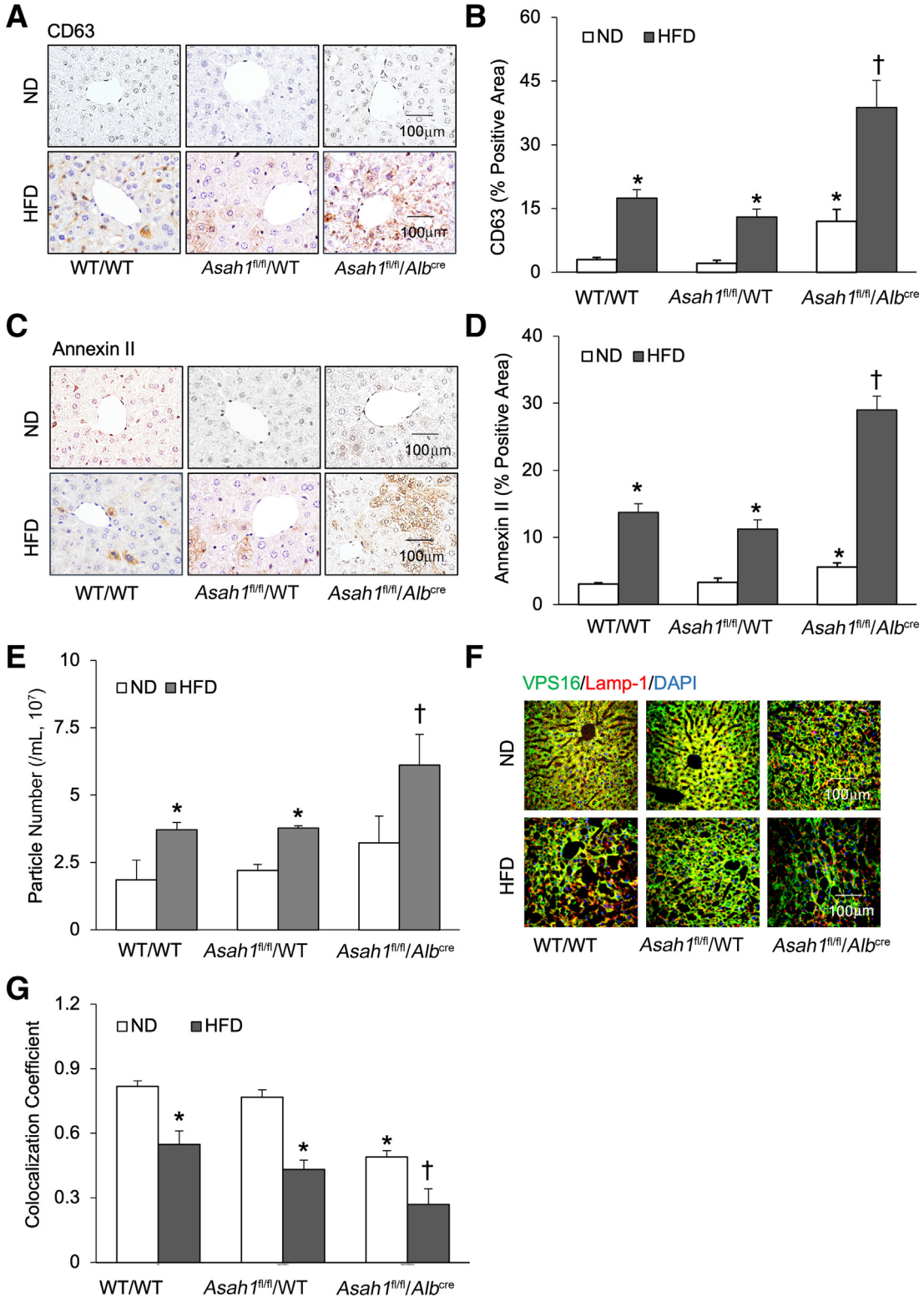

Figure 3 Enhanced extracellular vesicle (EV) release and attenuated interactions of multivesicular bodies with lysosomes by *Asah1* gene deletion in the liver of *Asah1*$^{fl/fl}$/*Alb*^{cre} mice on the high-fat diet (HFD). **A**–**D:** Representative immunohistochemistry staining and summarized data displaying the expression of EV marker CD63 and annexin II in the liver. **E:** Summarized data showing the relative concentration of plasma EVs released from the liver of different groups of mice. **F** and **G:** Representative images and summarized data showing the colocalization of vacuolar protein sorting-associated protein 16 homolog (VPS16) versus lysosomal-associated membrane protein-1 (Lamp-1) in the liver of different groups of mice. Data are expressed as means ± SEM (**B**, **D**, **E**, and **G**). $n = 5$ (**A**–**G**). *$P < 0.05$ versus wild-type (WT)/WT—normal diet (ND) or *Asah1*$^{fl/fl}$/WT-ND group; †$P < 0.05$ versus WT/WT—Western diet (WD) or *Asah1*$^{fl/fl}$/WT-HFD group. Scale bars = 100 μm (**A**, **C**, and **F**).

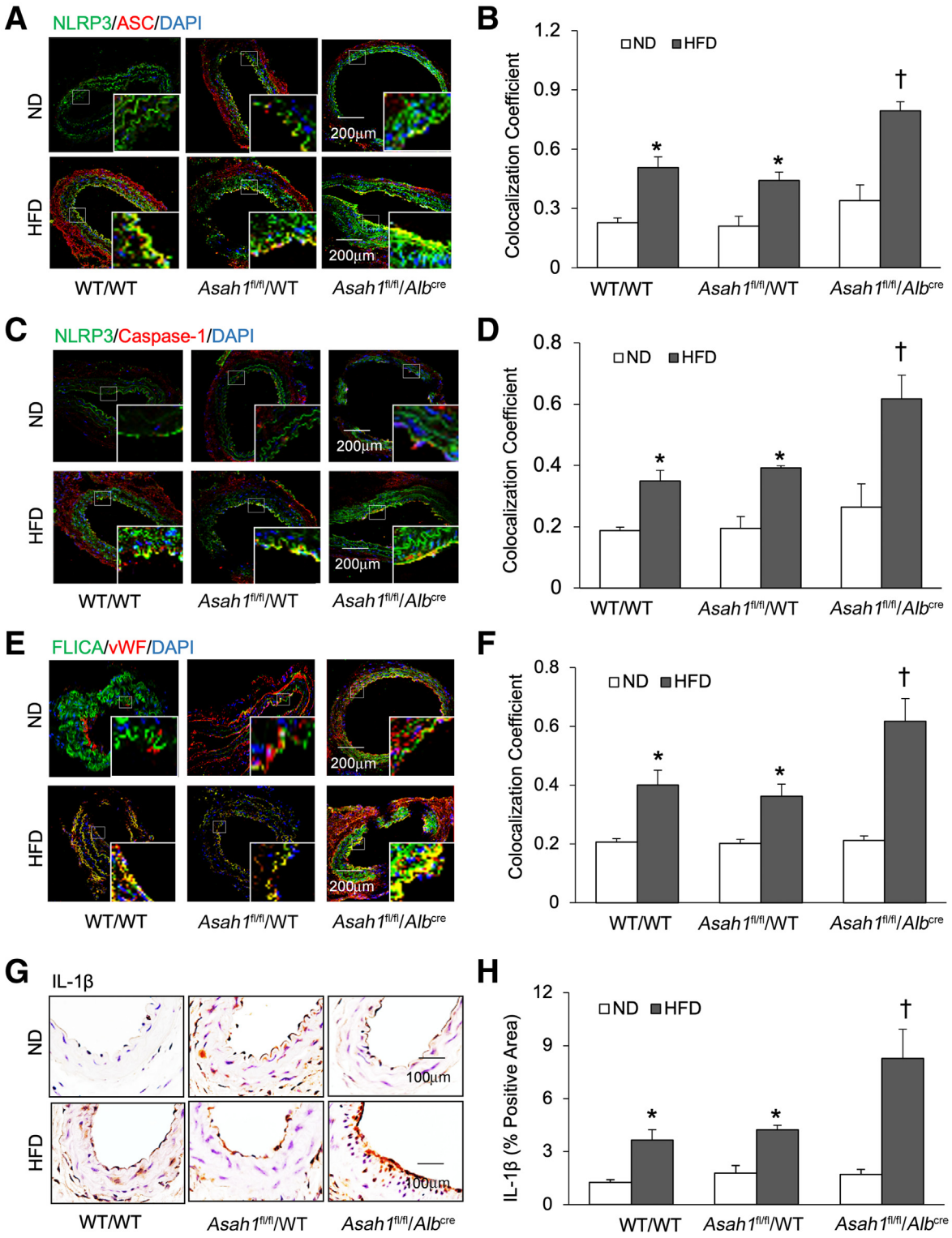

Figure 4 Enhanced endothelial Nod-like receptor pyrin domain 3 (NLRP3) inflammasome activation and formation in the carotid arterial wall by *Asah1* gene deletion in the liver of *Asah1*$^{fl/fl}$/*Alb*^{cre} mice on the high-fat diet (HFD). **A** and **C:** Representative fluorescent confocal microscope images, displaying the yellow dots or patches showing the colocalization of NLRP3 (green) versus ASC and caspase-1 (red). **B** and **D:** Summarized data showing the colocalization coefficient of NLRP3 versus apoptosis-associated speck-like protein containing a caspase activation and recruitment domain (ASC) and caspase-1. **E:** Representative fluorescent confocal microscope images showing the colocalization of fluorescent-labeled inhibitor of caspases (FLICA; green) with von Willebrand factor (vWF; red). **A**, **C**, and **E:** The **right corner boxed areas** represent amplified areas within the **small white boxed area**. **F:** Summarized data showing the colocalization coefficient of FLICA with vWF. **G:** Representative microscopic images of tissue slide with immunohistochemical staining showing IL-1β accumulation on the carotid arterial wall. **H:** Summarized data showing the density of IL-1β stained with selective anti—IL-1β antibody. Data are expressed as means ± SEM (**B**, **D**, **F**, and **H**). $n = 5$ (**A**—**H**). *$P < 0.05$ versus wild-type (WT)/WT—normal diet (ND) or *Asah1*$^{fl/fl}$/WT-ND group; †$P < 0.05$ versus WT/WT—Western diet (WD) or *Asah1*$^{fl/fl}$/WT-HFD group. Scale bars: 200 μm (**A**, **C**, and **E**); 100 μm (**G**).

and their control littermates. In contrast, Western diet significantly increased the neointima formation and intima/media ratio in PLCAs of WT/WT and *Asah1*$^{fl/fl}$/WT mice. The increase was significantly enhanced in *Asah1*$^{fl/fl}$/*Alb*^{cre} mice, as shown in the summarized data in Figure 5B. Moreover, using immunofluorescence microscopy, endothelial injury was detected by measuring the vWF expression in the carotid arteries. vWF is similarly expressed in ND-treated control (WT/WT and *Asah1*$^{fl/fl}$/WT) mice or *Asah1*$^{fl/fl}$/*Alb*^{cre} mice, showing the intact interendothelial vWF junction of carotid arteries. However, HFD significantly decreased vWF expression in the WT/WT and *Asah1*$^{fl/fl}$/WT mice, which was more pronounced in *Asah1*$^{fl/fl}$/*Alb*^{cre} mice (Figure 5, C and D). Together, these data suggest that increased hepatic steatosis by *Asah1* gene deletion leads to aggravated neointimal lesion formation and endothelial injury in carotid arteries.

Exaggerated Endothelial NLRP3 Inflammasome Activation and Formation by EVs Extracted from Mice Plasma of *Asah1*$^{fl/fl}$/*Alb*^{cre} Mice

EVs were purified and evaluated by flow cytometry of bead-coupled EVs after fluorescent immunolabeling for CD63 (Supplemental Figure S2A), nanoparticle tracking analysis (Supplemental Figure S2B), and Western blot analysis (Supplemental Figure S2C). The average peak size of EVs was 150 nm, determined by nanoparticle tracking analysis, and EVs express the typical markers CD63, CD9, and CD81, as well as CYP2E1, a liver cell marker. This indicates that some EVs are released from liver cells. Interestingly, CYP2E1 expression in the EVs from HFD mice was examined, and a significant increase was observed compared with the EVs from ND mice (Supplemental Figure S3). This result suggests that HFD contributed to the increase of EVs in the plasma, which may affect the functions of artery endothelial cells. Using stained EVs to co-culture with ECs, it was found that EVs from plasma easily entered ECs, as shown in Supplemental Figure S4.

Next, the effects of HFD-stimulated WT/WT and *Asah1*$^{fl/fl}$/EC^{cre} EVs were determined on the NLRP3 inflammasome formation and activation in ECs from carotid arteries (Figure 6). EVs were isolated from the plasma of WT/WT and *Asah1*$^{fl/fl}$/*Alb*^{cre} mice on the ND or HFD [ND-Exo (EVs isolated from plasma of mice on ND) or HFD-Exo (EVs isolated from plasma of mice on HFD), respectively], which were co-cultured with primary cultured endothelial cells from carotid arteries from WT/WT mice. As shown in Figure 6, A and B, the HFD-Exo from WT/WT mice dose dependently increased the expression of the cleaved

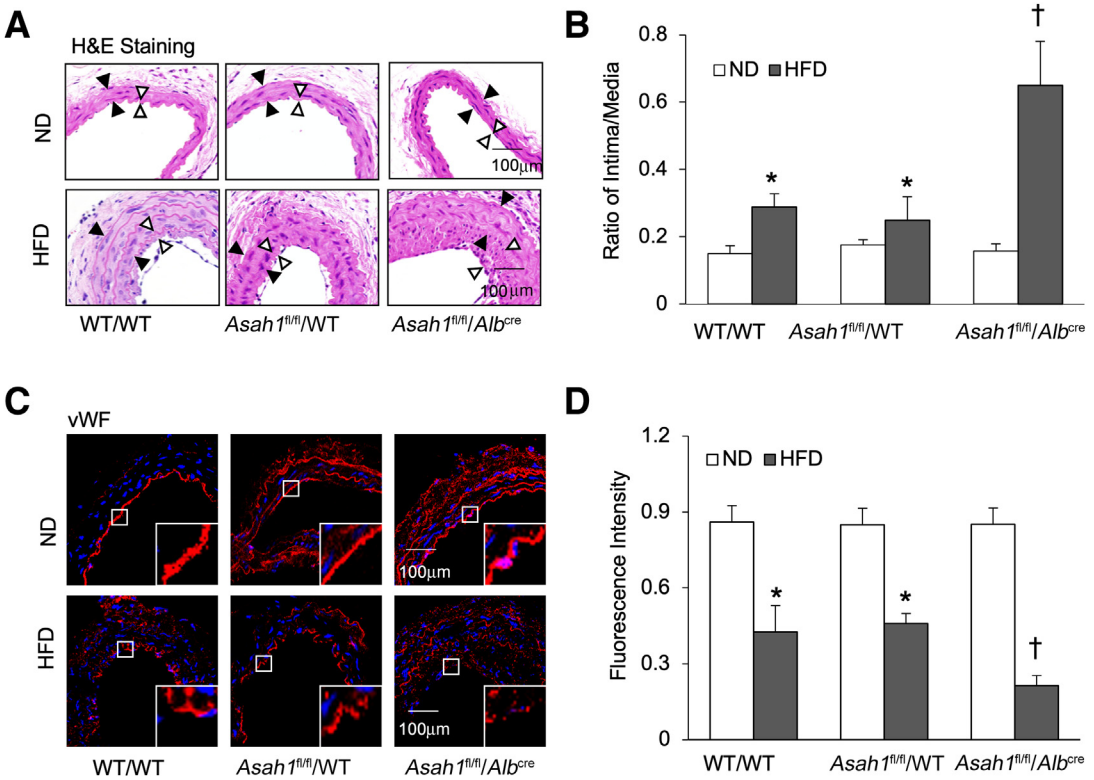

Figure 5 Enhanced neointima formation and endothelial injury in the carotid artery wall by *Asah1* gene deletion in the liver of *Asah1*$^{fl/fl}$/*Alb*^{cre} mice on the high-fat diet (HFD). **A:** Hematoxylin and eosin (H&E) staining showing the neointima and media in the mouse carotid arterial wall. The media area (**black arrowheads**) and the intima area (**white arrowheads**) are shown. **B:** Quantitative analysis of vascular lesions in partial ligated carotid artery, represented by calculation of the ratio between arterial intima and media area. **C:** Representative fluorescent confocal microscopic images showing the expression of von Willebrand factor (vWF). The **right corner boxed areas** represent amplified areas within the **small white boxed areas**. **D:** Summarized data showing the fluorescence intensity of vWF. Data are expressed as means ± SEM (**B** and **D**). $n = 5$ (**A**–**D**). *$P < 0.05$ versus wild-type (WT)/WT—normal diet (ND) or *Asah1*$^{fl/fl}$/WT-ND group; †$P < 0.05$ versus WT/WT—Western diet (WD) or *Asah1*$^{fl/fl}$/WT-HFD group. Scale bars = 100 μm (**A** and **C**).

caspase-1 expression in cultured endothelial cells when compared with untreated control cells. In contrast, no significant effects were found for ND-Exo from WT/WT or *Asah1*$^{fl/fl}$/EC^{cre} mice on endothelial cleaved caspase-1 expression, caspase-1 activity, or IL-1β production compared with the non-EV control cells. Interestingly, HFD-Exo from *Asah1*$^{fl/fl}$/EC^{cre} mice exhibited more potent effects than HFD-Exo from WT/WT mice on cleaved caspase-1 expression, caspase-1 activity, and IL-1β production (Figure 6, C–F). Consistently, by detecting the colocalization of NLPR3 with ASC or caspase-1, HFD-Exo from *Asah1*$^{fl/fl}$/EC^{cre} more significantly increased NLRP3 inflammasome assembly in ECs than HFD-Exo from WT/WT mice (Figure 7). Interestingly, pro–caspase-1 and cle–caspase-1 also were observed to be packaged in the EVs from mouse plasma (Supplemental Figure S5). These results suggest that EVs in the blood from the steatotic liver contributed to endothelial NLRP3 inflammasome activation and formation.

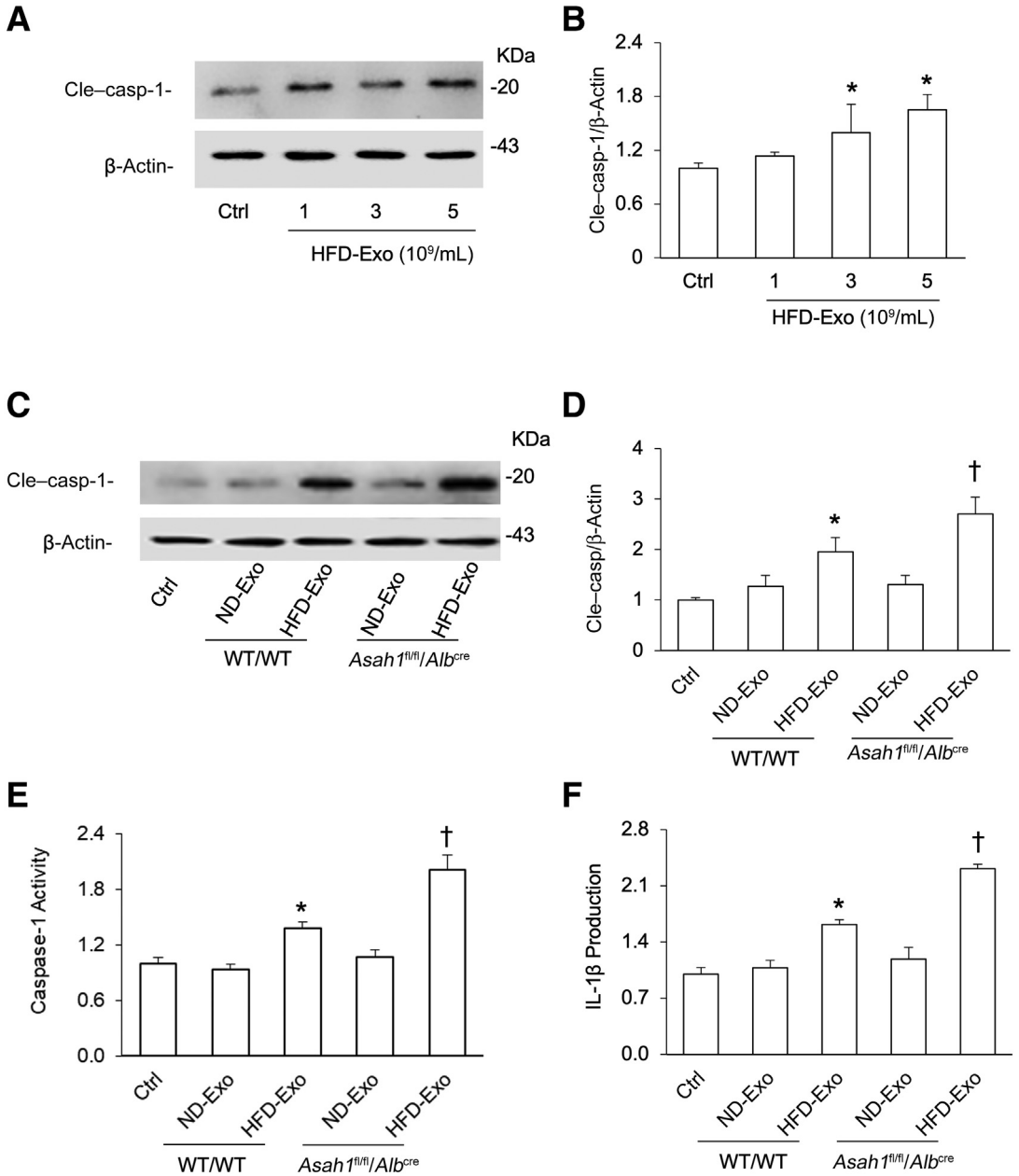

Figure 6 Exaggerated endothelial Nod-like receptor pyrin domain 3 inflammasome activation and IL-1β production by extracellular vesicles (EVs) extracted from mice plasma of *Asah1*$^{fl/fl}$/*Alb*^{cre} mice. **A:** Representative blots showing the dose effects of HFD-Exo [EVs isolated from plasma of mice on high-fat diet (HFD)] on the expression of cleaved caspase-1 (Cle–casp-1) compared with untreated controls (Ctrls). **B:** Summarized data showing the relative expression of cleaved caspase-1 induced by HFD-Exo. **C:** Representative blots showing the expression of cleaved caspase-1 induced by different EVs from the plasma of mice on normal diet (ND) or HFD. **D:** Summarized data showing the relative expression of cleaved caspase-1. **E:** Summarized data showing caspase-1 activity. **F:** Summarized data showing IL-1β production. Data are expressed as means ± SEM (**B** and **D**–**F**). $n = 5$ (**A**–**F**). *$P < 0.05$ versus wild-type (WT)/WT-ND or *Asah1*$^{fl/fl}$/WT-ND group; †$P < 0.05$ versus WT/WT–Western diet (WD) or *Asah1*$^{fl/fl}$/WT-HFD group. ND-Exo, EVs isolated from plasma of ND-treated mice.

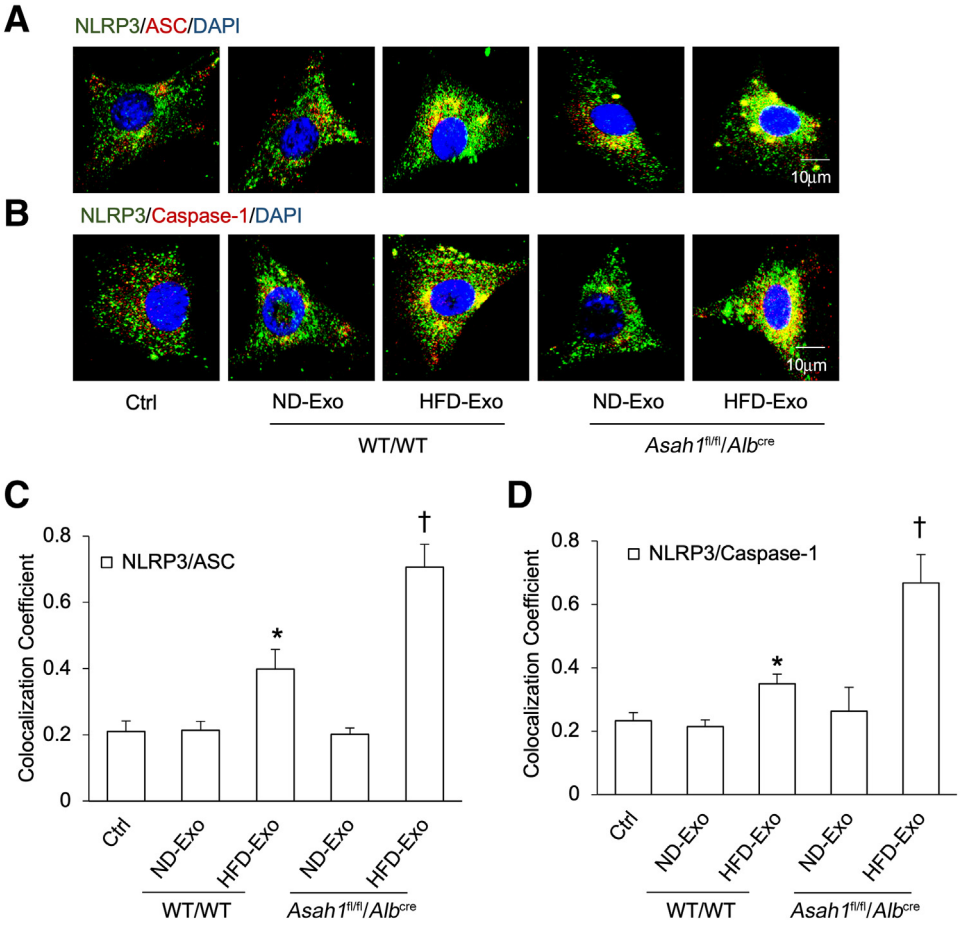

Figure 7 Exaggerated endothelial Nod-like receptor pyrin domain 3 (NLRP3) inflammasome formation by extracellular vesicles (EVs) extracted from plasma of *Asah1*$^{fl/fl}$/*Alb*^{cre} mice. **A** and **B:** Representative fluorescent confocal microscope images, displaying the yellow dots or patches showing the colocalization of NLRP3 (green) versus apoptosis-associated speck-like protein containing a caspase activation and recruitment domain (ASC) and caspase-1 (red). **C** and **D:** Summarized data showing the colocalization coefficient of NLRP3 versus ASC and caspase-1. Data are expressed as means ± SEM (**C** and **D**). $n = 5$ (**A**–**D**). *$P < 0.05$ versus wild-type (WT)/WT—normal diet (ND) or *Asah1*$^{fl/fl}$/WT-ND group; †$P < 0.05$ versus WT/WT—Western diet (WD) or *Asah1*$^{fl/fl}$/WT—high-fat diet (HFD) group. Scale bars = 10 μm (**A** and **B**). Ctrl, control; HFD-Exo, EVs isolated from plasma of HFD-treated mice; ND-Exo, EVs isolated from plasma of ND-treated mice.

Discussion

The current study explored the role of acid ceramidase/ceramide in hepatocyte-derived EV release and its contribution to hepatic steatosis—induced endothelial NLRP3 inflammasome activation, endothelial injury, and neointima formation. Lipid deposition and EV release were significantly enhanced in the liver of HFD-treated *Asah1*$^{fl/fl}$/*Alb*^{cre} mice compared with those in their littermates. This was accompanied by endothelial NLRP3 inflammasome activation and neointima formation as well as endothelial dysfunction in carotid arteries. Additionally, EVs isolated from the plasma of HFD-treated WT/WT mice increased NLRP3 inflammasome activation in endothelial cells *in vitro*, and the increases were enhanced by EVs from the plasma of HFD-treated *Asah1*$^{fl/fl}$/*Alb*^{cre} mice. The findings provide a novel insight into the important role for circulatory EVs in the interaction between the liver and the vascular system, suggesting a mechanistic link between NAFLD and vasculopathy associated with metabolic disorders.

An *Asah1* mutant mouse model, by flanking exon 1, has demonstrated that deletion of acid ceramidase signal peptide disrupts lysosomal targeting and activity of acid ceramidase, which causes ceramide accumulation in the lung, kidney, spleen, muscle, as well as liver.[43] To study the effects of *Asah1* mutant in NAFLD on CVDs, herein, *Asah1* floxed mice were crossed with albumin-Cre mice to generate liver-specific knockout mice (*Asah1*$^{fl/fl}$/*Alb*^{cre}). Characterization of *Asah1*$^{fl/fl}$/*Alb*^{cre} mice indicated that the deletion of acid ceramidase led to an accumulation of lysosomal ceramides in the liver. Although several mutations have been described in different domains of the *Asah1* enzyme, including two single base-pair mutations (Gln22His and His23Asp) in the signal peptide sequence,[44] reports on genotype-phenotype correlations are missing for most of the identified *Asah1* mutations. The present study, for the first time, reports the

Asah1$^{fl/fl}$/*Alb*^{cre} mice and the increase of lysosomal ceramides, which is seminal to offering further insights into the pathogenesis of ceramide-associated diseases.

Among the many identified factors, ceramide accumulation contributes to both NAFLD and alcoholic liver disease in various models. Kasumov et al[21] have reported that inhibition of ceramide synthesis is associated with a profound reversal of diet-induced hepatic steatosis and inflammation, suggesting that modulation of ceramide synthesis may lead to the development of novel strategies for the treatment of both NAFLD and its associated atherosclerosis. Moreover, pharmacologic ceramide reduction has been reported to alleviate alcohol-induced steatosis and hepatomegaly in adiponectin knockout mice.[45] Recently, Correnti et al[46] have demonstrated that hepatic ceramide reduction ameliorates the effects of alcohol on hepatic lipid droplet accumulation by promoting very low-density lipoprotein secretion and lipophagy, the latter of which involves ceramide cross talk between the lysosomal and lipid droplet compartments. In the current study, a mouse model of NAFLD with HFD was established. HFD successfully induced steatosis in the control (WT/WT or *Asah1*$^{fl/fl}$/WT) mice, as shown by increased lipid droplet accumulation in the liver, whereas *Asah1*$^{fl/fl}$/*Alb*^{cre} mice on HFD had more severe steatosis compared with control mice. The severity of the steatosis correlated well with the hepatic ceramide levels as a higher ceramide level was observed in *Asah1*$^{fl/fl}$/*Alb*^{cre} mice compared with that in control mice. These data are consistent with previous relative studies and suggest that deletion of acid ceramidase causes lysosomal ceramide accumulation, which contributes to mouse NAFLD in the liver.

In recent years, EVs or exosomes have emerged as critical mediators in the intercellular communication and between the interactions of cell-cell or organ-organ communications, which play important roles in the various pathophysiological processes.[47,48] EVs can be released into extracellular fluid and circulation by various types of cells, such as macrophages, hepatocytes, adipocytes, and many others. The number and overall composition of EVs released by donor cells are often altered in response to various stresses or pathologic stimuli. For instance, hepatocytes under lipotoxic stress have been shown to dramatically increase the release of EVs.[49,50] Previous studies have shown that excessive lipids stimulate the release of hepatocytes-EVs with proinflammatory molecules inside.[51,52] Momen-Heravi et al[53] showed that alcohol-treated hepatocytes release exosomes, which carry miRNA-122, to enhance the inflammatory response in monocytes and affect their immune function. In alcoholic liver disease, alcohol-exposed human monocytes can release exosomes, which can subsequently stimulate the polarization of naive monocytes, then form M2 macrophages.[53] In a hepatitis C virus–induced fibrosis model, exosomes released by hepatitis C virus–infected hepatocytes carry miR-19a, which can be internalized by hepatic stellate cells.[54] Previous studies have demonstrated that lysosomal ceramide plays an important role in regulating exosome release in different types of cells, including smooth muscle cells,[35,55] podocytes,[56] and endothelial cells.[29] Herein, it was demonstrated that *Asah1* gene deletion significantly augmented the HFD-induced release of hepatic EVs and reduction in the lysosome interaction with MVBs. The precise molecular mechanisms by which lysosomal ceramide regulates exosomal release remain unknown and are worth future investigation. Nonetheless, the results from the present study support the view that lysosomal ceramide accumulation due to acid ceramidase deficiency contributes to the pathogenesis of steatosis and impairs lysosomal fusion with MVBs, leading to intensified hepatic EV release.

Recent studies have shown that hepatocyte-derived exosomes carrying hepatocyte-specific contents can easily pass through the sinusoidal endothelium.[57,58] They stimulate various nonparenchymal cells, including monocytes,[53] lymphocytes,[59] hepatic stellate cells,[60,61] and endothelial cells,[62] which play an important role in signaling transmission. Recently, it has been demonstrated that hepatocyte-derived exosomes/EVs promote endothelial inflammation and facilitate atherogenesis by miR-1 delivery, Kruppel-like factor 4 (KLF4) suppression, and NF-κB activation, which illustrates an important role of hepatocyte-derived exosomes in distant communications between the liver and vasculature.[14] Increasing evidence has shown that exosomes are the upstream regulators for inflammasome activation, although some studies have demonstrated that inflammasome activation could regulate the release of exosomes.[63] Interestingly, most reports have elucidated that exosomes from stem cells, such as adipose tissue–derived mesenchymal stem cells, bone marrow–derived stem cells, and embryonic stem cells, always show their inhibitor effects on inflammasome activation. However, exosomes isolated from other cells show the opposite data, indicating the positive correlation between exosomal release and inflammasome activation. Especially, Kerr et al[64] reported that delivery of serum-derived EVs to human microvascular endothelial cells activated the inflammasome and resulted in endothelial cell pyroptosis. Previous studies have demonstrated that HFD induces neointimal formation in partial ligated carotid arteries, which was attributed, at least in part, to endothelial NLRP3 inflammasome activation and consequent endothelial damage.[65] In the present study, it was observed that intensified hepatic EV release in *Asah1*$^{fl/fl}$/*Alb*^{cre} mice was correlated with aggravated NLRP3 inflammasome activation, endothelial injury, and neointimal formation. In *in vitro* studies, it was further demonstrated that EVs isolated from HFD-treated WT/WT mice dose dependently increased NLRP3 inflammasome activation in cultured ECs, and such inflammasome-activating effects were only observed for EVs from HFD-treated WT/WT or *Asah1*$^{fl/fl}$/*Alb*^{cre} mice but not from ND-treated mice. Together, the findings from *in vivo* and *in vitro* studies support the view that hepatic EVs released from the steatotic liver directly activate

endothelial NLRP3 inflammasomes and thereby contribute to endothelial injury and neointimal formation. When ECs were stimulated with the same amounts of EVs, the EVs isolated from HFD-treated *Asah1*$^{fl/fl}$/*Alb*^{cre} mice exhibited more potent activating effects on endothelial NLRP3 inflammasomes than those from WT/WT mice. This difference could be due to changes either in their cargos (eg, miRNAs) or membrane components (eg, ceramides), which deserve further investigations.

In summary, the present study demonstrated that *Asah1* gene deficiency in the liver results in lysosomal ceramide increase, leading to enhancement of HFD-induced hepatic steatosis and EV release, which causes the carotid endothelial dysfunction through endothelial NLRP3 inflammasome formation and activation. The authors' results provide novel insights into understanding the novel role of circulatory EVs in linking NAFLD and vasculopathy in metabolic disorders.

Supplemental Data

Supplemental material for this article can be found at *http://doi.org/10.1016/j.ajpath.2022.12.007*.

References

1. Idalsoaga F, Kulkarni AV, Mousa OY, Arrese M, Arab JP: Non-alcoholic fatty liver disease and alcohol-related liver disease: two intertwined entities. Front Med (Lausanne) 2020, 7:448
2. Arvind A, Henson JB, Osganian SA, Nath C, Steinhagen LM, Memel ZN, Donovan A, Balogun O, Chung RT, Simon TG, Corey KE: Risk of cardiovascular disease in individuals with non-obese nonalcoholic fatty liver disease. Hepatol Commun 2022, 6: 309−319
3. Targher G, Corey KE, Byrne CD: NAFLD, and cardiovascular and cardiac diseases: factors influencing risk, prediction and treatment. Diabetes Metab 2021, 47:101215
4. Lu HY, Liu H, Hu F, Zou LL, Luo SK, Sun L: Independent association between nonalcoholic fatty liver disease and cardiovascular disease: a systematic review and meta-analysis. Int J Endocrinol 2013, 2013:124958
5. Ballestri S, Lonardo A, Bonapace S, Byrne CD, Loria P, Targher G: Risk of cardiovascular, cardiac and arrhythmic complications in patients with non-alcoholic fatty liver disease. World J Gastroenterol 2014, 20:1724−1745
6. Dogru T, Genc H, Tapan S, Ercin CN, Ors F, Aslan F, Kara M, Sertoglu E, Bagci S, Kurt I, Sonmez A: Elevated asymmetric dimethylarginine in plasma: an early marker for endothelial dysfunction in non-alcoholic fatty liver disease? Diabetes Res Clin Pract 2012, 96: 47−52
7. Cunningham RP, Sheldon RD, Rector RS: The emerging role of hepatocellular eNOS in non-alcoholic fatty liver disease development. Front Physiol 2020, 11:767
8. Hwang HW, Yu JH, Jin YJ, Suh YJ, Lee JW: Correlation between the small dense LDL level and nonalcoholic fatty liver disease: possibility of a new biomarker. Medicine (Baltimore) 2020, 99:e21162
9. Kitade H, Chen GL, Ni YH, Ota T: Nonalcoholic fatty liver disease and insulin resistance: new insights and potential new treatments. Nutrients 2017, 9:387
10. Wang XX, Rao HY, Liu F, Wei L, Li HG, Wu CD: Recent advances in adipose tissue dysfunction and its role in the pathogenesis of non-alcoholic fatty liver disease. Cells 2021, 10:3300
11. Hadi HAR, Carr CS, Al Suwaidi J: Endothelial dysfunction: cardiovascular risk factors, therapy, and outcome. Vasc Health Risk Manag 2005, 1:183−198
12. Zheng Y, Wang JR, Zhao TJ, Wang L, Wang JH: Modulation of the VEGF/AKT/eNOS signaling pathway to regulate liver angiogenesis to explore the anti-hepatic fibrosis mechanism of curcumol. J Ethnopharmacol 2021, 280:114480
13. Vourakis M, Mayer G, Rousseau G: The role of gut microbiota on cholesterol metabolism in atherosclerosis. Int J Mol Sci 2021, 22: 8074
14. Jiang FJ, Chen Q, Wang W, Ling Y, Yan Y, Xia P: Hepatocyte-derived extracellular vesicles promote endothelial inflammation and atherogenesis via microRNA-1. J Hepatol 2020, 72:156−166
15. Xu R, Rai A, Chen MS, Suwakulsiri W, Greening DW, Simpson RJ: Extracellular vesicles in cancer - implications for future improvements in cancer care. Nat Rev Clin Oncol 2018, 15:617−638
16. Wolf P: The nature and significance of platelet products in human plasma. Br J Haematol 1967, 13:269−288
17. Han C, Yang J, Sun J, Qin G: Extracellular vesicles in cardiovascular disease: biological functions and therapeutic implications. Pharmacol Ther 2021, 233:108025
18. Zuo R, Ye LF, Huang Y, Song ZQ, Wang L, Zhi H, Zhang MY, Li JY, Zhu L, Xiao WJ, Shang HC, Zhang Y, He RR, Chen Y: Hepatic small extracellular vesicles promote microvascular endothelial hyperpermeability during NAFLD via novel-miRNA-7. J Nanobiotechnology 2021, 19:396
19. Hajduch E, Lachkar F, Ferre P, Foufelle F: Roles of ceramides in non-alcoholic fatty liver disease. J Clin Med 2021, 10:792
20. Jiang M, Li C, Liu QS, Wang AM, Lei MX: Inhibiting ceramide synthesis attenuates hepatic steatosis and fibrosis in rats with non-alcoholic fatty liver disease. Front Endocrinol (Lausanne) 2019, 10:665
21. Kasumov T, Li L, Li M, Gulshan K, Kirwan JP, Liu XL, Previs S, Willard B, Smith JD, McCullough A: Ceramide as a mediator of non-alcoholic fatty liver disease and associated atherosclerosis. PLoS One 2015, 10:e0126910
22. Li GB, Huang DD, Hong JN, Bhat OM, Yuan XX, Li PL: Control of lysosomal TRPML1 channel activity and exosome release by acid ceramidase in mouse podocytes. Am J Physiol Cell Physiol 2019, 317:C481−C491
23. Ni J, Zhang X, Li J, Zheng Z, Zhang J, Zhao W, Liu L: Tumour-derived exosomal lncRNA-SOX2OT promotes bone metastasis of non-small cell lung cancer by targeting the miRNA-194-5p/RAC1 signalling axis in osteoclasts. Cell Death Dis 2021, 12:662
24. Bhat OM, Li GB, Yuan XX, Huang DD, Gulbins E, Kukreja RC, Li PL: Arterial medial calcification through enhanced small extracellular vesicle release in smooth muscle-specific Asah1 gene knockout mice. Sci Rep 2020, 10:1645
25. Bhat OM, Yuan XX, Lohner H, Li PL: Lysosome dysfunction and medial calcification in the arterial wall of smooth muscle cell-specific Smpd1 transgenic mice: a ceramide-mediated vasculopathy. FASEB J 2019, 33:679.13
26. Committee for the Update of the Guide for the Care and Use of Laboratory Animals; National Research Council: Guide for the Care and Use of Laboratory Animals. Eighth Edition. Washington, DC, National Academies Press, 2011
27. Yuan X, Wang L, Bhat OM, Lohner H, Li PL: Differential effects of short chain fatty acids on endothelial Nlrp3 inflammasome activation and neointima formation: antioxidant action of butyrate. Redox Biol 2018, 16:21−31
28. Yuan X, Bhat OM, Lohner H, Li N, Zhang Y, Li PL: Inhibitory effects of growth differentiation factor 11 on autophagy deficiency-induced dedifferentiation of arterial smooth muscle cells. Am J Physiol Heart Circ Physiol 2019, 316:H345−H356

29. Yuan X, Bhat OM, Lohner H, Zhang Y, Li PL: Endothelial acid ceramidase in exosome-mediated release of NLRP3 inflammasome products during hyperglycemia: evidence from endothelium-specific deletion of Asah1 gene. Biochim Biophys Acta Mol Cell Biol Lipids 2019, 1864:158532
30. Abraham NG, Sodhi K, Silvis AM, Vanella L, Favero G, Rezzani R, Lee C, Zeldin DC, Schwartzman ML: CYP2J2 targeting to endothelial cells attenuates adiposity and vascular dysfunction in mice fed a high-fat diet by reprogramming adipocyte phenotype. Hypertension 2014, 64:1352−1361
31. Li X, Zhang Y, Xia M, Gulbins E, Boini KM, Li PL: Activation of Nlrp3 inflammasomes enhances macrophage lipid-deposition and migration: implication of a novel role of inflammasome in atherogenesis. PLoS One 2014, 9:e87552
32. Zhang C, Yi F, Xia M, Boini KM, Zhu Q, Laperle LA, Abais JM, Brimson CA, Li PL: NMDA receptor-mediated activation of NADPH oxidase and glomerulosclerosis in hyperhomocysteinemic rats. Antioxid Redox Signal 2010, 13:975−986
33. Koka S, Xia M, Chen Y, Bhat OM, Yuan X, Boini KM, Li PL: Endothelial NLRP3 inflammasome activation and arterial neointima formation associated with acid sphingomyelinase during hypercholesterolemia. Redox Biol 2017, 13:336−344
34. Kapustin AN, Chatrou ML, Drozdov I, Zheng Y, Davidson SM, Soong D, Furmanik M, Sanchis P, De Rosales RT, Alvarez-Hernandez D, Shroff R, Yin X, Muller K, Skepper JN, Mayr M, Reutelingsperger CP, Chester A, Bertazzo S, Schurgers LJ, Shanahan CM: Vascular smooth muscle cell calcification is mediated by regulated exosome secretion. Circ Res 2015, 116:1312−1323
35. Yuan X, Bhat OM, Samidurai A, Das A, Zhang Y, Li PL: Reversal of endothelial extracellular vesicle-induced smooth muscle phenotype transition by hypercholesterolemia stimulation: role of NLRP3 inflammasome activation. Front Cell Dev Biol 2020, 8:597423
36. Li X, Han WQ, Boini KM, Xia M, Zhang Y, Li PL: TRAIL death receptor 4 signaling via lysosome fusion and membrane raft clustering in coronary arterial endothelial cells: evidence from ASM knockout mice. J Mol Med (Berl) 2013, 91:25−36
37. Kobayashi M, Inoue K, Warabi E, Minami T, Kodama T: A simple method of isolating mouse aortic endothelial cells. J Atheroscler Thromb 2005, 12:138−142
38. Dong H, Huang H, Yun X, Kim DS, Yue Y, Wu H, Sutter A, Chavin KD, Otterbein LE, Adams DB, Kim YB, Wang H: Bilirubin increases insulin sensitivity in leptin-receptor deficient and diet-induced obese mice through suppression of ER stress and chronic inflammation. Endocrinology 2014, 155:818−828
39. Yuan X, Bhat OM, Meng N, Lohner H, Li PL: Protective role of autophagy in Nlrp3 inflammasome activation and medial thickening of mouse coronary arteries. Am J Pathol 2018, 188:2948−2959
40. Eitan E, Suire C, Zhang S, Mattson MP: Impact of lysosome status on extracellular vesicle content and release. Ageing Res Rev 2016, 32:65−74
41. Park JH, Schuchman EH: Acid ceramidase and human disease. Biochim Biophys Acta 2006, 1758:2133−2138
42. Laurier-Laurin ME, De Montigny A, Attiori Essis S, Cyr M, Massicotte G: Blockade of lysosomal acid ceramidase induces GluN2B-dependent Tau phosphorylation in rat hippocampal slices. Neural Plast 2014, 2014:196812
43. Beckmann N, Kadow S, Schumacher F, Gothert JR, Kesper S, Draeger A, Schulz-Schaeffer WJ, Wang J, Becker JU, Kramer M, Kuhn C, Kleuser B, Becker KA, Gulbins E, Carpinteiro A: Pathological manifestations of Farber disease in a new mouse model. Biol Chem 2018, 399:1183−1202
44. Zhang Z, Mandal AK, Mital A, Popescu N, Zimonjic D, Moser A, Moser H, Mukherjee AB: Human acid ceramidase gene: novel mutations in Farber disease. Mol Genet Metab 2000, 70:301−309
45. Correnti JM, Juskeviciute E, Swarup A, Hoek JB: Pharmacological ceramide reduction alleviates alcohol-induced steatosis and hepatomegaly in adiponectin knockout mice. Am J Physiol Gastrointest Liver Physiol 2014, 306:G959−G973
46. Correnti J, Lin C, Brettschneider J, Kuriakose A, Jeon S, Scorletti E, Oranu A, McIver-Jenkins D, Kaneza I, Buyco D, Saiman Y, Furth EE, Argemi J, Bataller R, Holland WL, Carr RM: Liver-specific ceramide reduction alleviates steatosis and insulin resistance in alcohol-fed mice. J Lipid Res 2020, 61:983−994
47. Mathieu M, Martin-Jaular L, Lavieu G, Thery C: Specificities of secretion and uptake of exosomes and other extracellular vesicles for cell-to-cell communication. Nat Cell Biol 2019, 21:9−17
48. Maas SLN, Breakefield XO, Weaver AM: Extracellular vesicles: unique intercellular delivery vehicles. Trends Cell Biol 2017, 27:172−188
49. Novotny V, Miller SE, Hrcek J, Baje L, Basset Y, Lewis OT, Stewart AJ, Weiblen GD: Insects on plants: explaining the paradox of low diversity within specialist herbivore guilds. Am Nat 2012, 179:351−362
50. Fukushima M, Dasgupta D, Mauer AS, Kakazu E, Nakao K, Malhi H: StAR-related lipid transfer domain 11 (STARD11)-mediated ceramide transport mediates extracellular vesicle biogenesis. J Biol Chem 2018, 293:15277−15289
51. Hirsova P, Ibrahim SH, Krishnan A, Verma VK, Bronk SF, Werneburg NW, Charlton MR, Shah VH, Malhi H, Gores GJ: Lipid-induced signaling causes release of inflammatory extracellular vesicles from hepatocytes. Gastroenterology 2016, 150:956−967
52. Liao CY, Song MJ, Gao Y, Mauer AS, Revzin A, Malhi H: Hepatocyte-derived lipotoxic extracellular vesicle sphingosine 1-phosphate induces macrophage chemotaxis. Front Immunol 2018, 9:2980
53. Momen-Heravi F, Bala S, Kodys K, Szabo G: Exosomes derived from alcohol-treated hepatocytes horizontally transfer liver specific miRNA-122 and sensitize monocytes to LPS. Sci Rep 2015, 5:9991
54. Devhare PB, Sasaki R, Shrivastava S, Di Bisceglie AM, Ray R, Ray RB: Exosome mediated intercellular communication between hepatitis C virus-infected hepatocytes and hepatic stellate cells. J Virol 2017, 91:e02225-16
55. Bhat OM, Yuan X, Kukreja RC, Li PL: Regulatory role of mammalian target of rapamycin signaling in exosome secretion and osteogenic changes in smooth muscle cells lacking acid ceramidase gene. FASEB J 2021, 35:e21732
56. Ni S, Ling Z, Wang X, Cao Y, Wu T, Deng R, Crane JL, Skolasky R, Demehri S, Zhen G, Jain A, Wu P, Pan D, Hu B, Lyu X, Li Y, Chen H, Qi H, Guan Y, Dong X, Wan M, Zou X, Lu H, Hu J, Cao X: Sensory innervation in porous endplates by Netrin-1 from osteoclasts mediates PGE2-induced spinal hypersensitivity in mice. Nat Commun 2019, 10:5643
57. Wetmore BA, Brees DJ, Singh R, Watkins PB, Andersen ME, Loy J, Thomas RS: Quantitative analyses and transcriptomic profiling of circulating messenger RNAs as biomarkers of rat liver injury. Hepatology 2010, 51:2127−2139
58. Conde-Vancells J, Rodriguez-Suarez E, Embade N, Gil D, Matthiesen R, Valle M, Elortza F, Lu SC, Mato JM, Falcon-Perez JM: Characterization and comprehensive proteome profiling of exosomes secreted by hepatocytes. J Proteome Res 2008, 7:5157−5166
59. Cobb DA, Kim OK, Golden-Mason L, Rosen HR, Hahn YS: Hepatocyte-derived exosomes promote T follicular regulatory cell expansion during hepatitis C virus infection. Hepatology 2018, 67:71−85
60. Seo W, Eun HS, Kim SY, Yi HS, Lee YS, Park SH, Jang MJ, Jo E, Kim SC, Han YM, Park KG, Jeong WI: Exosome-mediated activation of toll-like receptor 3 in stellate cells stimulates interleukin-17 production by gammadelta T cells in liver fibrosis. Hepatology 2016, 64:616−631
61. Chen L, Chen R, Kemper S, Charrier A, Brigstock DR: Suppression of fibrogenic signaling in hepatic stellate cells by Twist1-dependent microRNA-214 expression: role of exosomes in horizontal transfer of Twist1. Am J Physiol Gastrointest Liver Physiol 2015, 309:G491−G499
62. Giugliano S, Kriss M, Golden-Mason L, Dobrinskikh E, Stone AE, Soto-Gutierrez A, Mitchell A, Khetani SR, Yamane D, Stoddard M, Li H,

Shaw GM, Edwards MG, Lemon SM, Gale M Jr, Shah VH, Rosen HR: Hepatitis C virus infection induces autocrine interferon signaling by human liver endothelial cells and release of exosomes, which inhibits viral replication. Gastroenterology 2015, 148:392−402.e13

63. Noonin C, Thongboonkerd V: Exosome-inflammasome crosstalk and their roles in inflammatory responses. Theranostics 2021, 11:4436−4451

64. Kerr NA, de Rivero Vaccari JP, Umland O, Bullock MR, Conner GE, Dietrich WD, Keane RW: Human lung cell pyroptosis following traumatic brain injury. Cells 2019, 8:69

65. Xia M, Boini KM, Abais JM, Xu M, Zhang Y, Li PL: Endothelial NLRP3 inflammasome activation and enhanced neointima formation in mice by adipokine visfatin. Am J Pathol 2014, 184:1617−1628